International Journal of Fracture **58:** 137–156, 1992.
© 1992 *Kluwer Academic Publishers. Printed in the Netherlands.*

A finite element investigation of quasi-static and dynamic asymptotic crack-tip fields in hardening elastic-plastic solids under plane stress
Part II: Crack growth in power-law hardening materials

XIAOMIN DENG* and ARES J. ROSAKIS
*California Institute of Technology, Pasadena, California 91125, USA; (*now at the Department of Mechanical Engineering, University of South Carolina, Columbia, South Carolina 29208, USA)*

Received 20 July 1990; accepted in revised form 11 May 1992

Abstract. This is the second half of a two-part finite element investigation of quasi-static and dynamic crack growth in hardening elastic-plastic solids under mode I plane stress, steady state, and small-scale yielding conditions. The hardening materials are assumed to obey the von Mises yield criterion and the associated flow rule, and are characterized by a Ramberg-Osgood type power-law effective stress-strain curve. The asymptotic feature of the crack-tip stress and deformation fields, and the influence of hardening and crack propagation speed on these fields as well as on the size and shape of the crack-tip active plastic zone, are addressed in detail. The results of this study strongly suggest the existence of stress and strain singularities of the type $[\ln(R_0/r)]^s$ ($s > 0$) at $r = 0$, where r is the distance to the crack tip and R_0 is a length scaling parameter, which is consistent with the predictions of asymptotic analyses of variable-separable type by Gao et al. [1–4]. Difficulties in estimating the values of R_0 and s by fitting the results of the present full-field study to the type of singularities shown above are analyzed, and quantitative differences between the results of this study and those of the asymptotic analyses are discussed. As expected, findings presented here share many similarities with those reported in the first part of this study [5] for crack growth in linear hardening solids. A prominent common feature of crack growth in these two types of hardening materials is that as the level of hardening decreases and the crack propagation speed increases, a secondary yield zone emerges along the crack surface, and kinks in the angular variations of the stress and velocity fields begin to develop near where elastic unloading is taking place.

1. Introduction

This part of the study is concerned with quasi-static and dynamic crack growth under mode I plane stress, steady state, and small-scale yielding conditions, in power-law hardening elastic-plastic materials which are homogeneous and isotropic, and obey the von Mises yield condition and the associated flow rule. The effective stress-strain curve of the materials is assumed to follow a uniaxial stress-strain relation of the Ramberg-Osgood type:

$$\sigma = \begin{cases} E\varepsilon, & \text{if } \sigma \leqslant \sigma_0; \\ \sigma_0(\varepsilon/\varepsilon_0)^{1/n}, & \text{if } \sigma \geqslant \sigma_0, \end{cases}$$

where E is the Young's modulus; σ_0 and $\varepsilon_0 = \sigma_0/E$ are the initial yield stress and strain, respectively, in tension; and n ($1 \leqslant n \leqslant \infty$) is the hardening exponent. When n is set to one, the above relation models a linearly elastic material, and at the limit $n \to \infty$, the elastic-perfectly plastic case is recovered.

For isotropic power-law hardening elastic-plastic solids, asymptotic analyses of steady-state, quasi-static crack growth were performed by Gao, Zhang and Hwang [1] under mode III conditions and by Gao and Hwang [2] under mode I plane strain conditions. After exploring the possibility of variable-separable solutions with logarithmic and power series expansions, they concluded that the near-tip stress and plastic strain singularities are of the logarithmic type.

Their analyses show that as the distance to the crack tip r approaches zero, the stresses are as singular as $[\ln(R_0/r)]^{2/(n-1)}$ in mode III, and as $[\ln(R_0/r)]^{1/(n-1)}$ in mode I plane strain, where n ($n > 1$) is the hardening exponent and R_0 is a length scaling parameter not obtainable asymptotically. The singularities of the strain components are slightly more complex: In mode III, ε_{31} is as singular as $[\ln(R_0/r)]^{(n+1)/(n-1)}$ and ε_{32} is as singular as $[\ln(R_0/r)]^{2n/(n-1)}$, and in mode I plane strain all strain components are as singular as $[\ln(R_0/r)]^{n/(n-1)}$. It must be pointed out that there is as yet no similar asymptotic analysis for quasi-static crack growth under mode I plane stress conditions.

For dynamic crack propagation in isotropic power-law hardening solids, similar steady-state asymptotic analyses were conducted by Gao and Nemat-Nasser [3] under mode III and mode I and II plane strain conditions (for imcompressible materials only), and by Zhang and Gao [4] under mode I plane stress conditions. By assuming certain forms of variable-separable displacement expansions, these researchers were able to draw conclusions regarding the singularities of the crack-tip stress and strain fields. Unlike the case of quasi-static crack growth, the stress and strain fields during dynamic crack growth have singularities of the type $[\ln(R_0/r)]^{1/(n-1)}$ and $[\ln(R_0/r)]^{n/(n-1)}$, respectively, for all three fracture modes. Furthermore, they argued that the angular stress and strain variations for mode I and II dynamic crack growth in power-law hardening solids are the same as those in elastic-perfectly plastic materials.

While asymptotic analyses of crack growth in power-law hardening solids abound, corresponding full-field numerical investigations of asymptotic crack-tip fields are rare. In fact, to the present authors' knowledge, there is no full-field numerical analysis of dynamic crack propagation regarding the nature of the crack-tip fields and their dependence on hardening and crack speed. However, steady progress has been made in this area, and under quasi-static conditions, several finite element studies have been reported in the literature.

The first finite element computation was carried out by Dean and Hutchinson [6]. They considered quasi-static crack growth under mode III and mode I plane strain, steady state, and small-scale yielding conditions in isotropic hardening materials as well as anisotropic hardening solids characterized by a J_2 corner theory of plasticity [7]. Results gave the shape of the crack-tip active plastic zone, the variation of the crack opening displacement, and the distribution of strains at the front of the crack tip.

A more detailed finite element investigation of steady-state, quasi-static crack growth was later conducted by Lam [8] under mode I plane strain conditions and for isotropic hardening solids. Angular variations of the stress and plastic strain fields, as well as the radial variations of the hoop stress component, were addressed in this study.

A similar finite element analysis was provided by Luo, Zhang and Hwang [9] for steady-state, quasi-static crack growth in mode I plane stress. Results were presented for the variations of the crack-tip active plastic zone with respect to the power-law hardening exponent.

It is noted that the above numerical studies all employed an Eulerian type finite element formulation first used by Dean and Hutchinson [6]. A nodal release procedure [10] was adopted in a more recent finite element investigation by Narasimhan, Rosakis and Hall [11]. Stable crack growth was modelled in this study by gradually separating the crack tip node according to a presumed fracture criterion. Findings are reported for the shape of the crack-tip active plastic zone, the crack opening displacement, angular stress variations, radial stress and plastic strain distributions ahead of the crack tip.

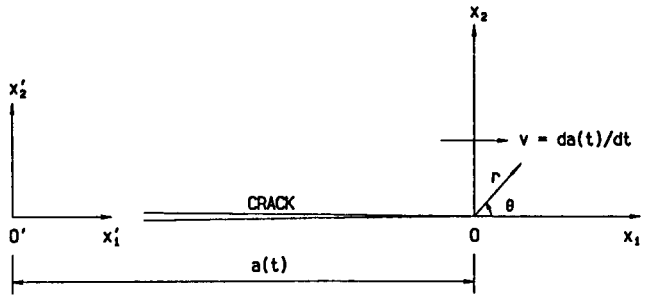

Fig. 1.1. A diagram of crack propagation, where (x_1', x_2') is a fixed reference coordinate system; (x_1, x_2) is a moving system with origin at the crack tip; and (r, θ) is the associated polar coordinate system.

The above analytical and numerical studies provide a basis for the present investigation, and the results of these studies will be discussed and compared with ours whenever possible and appropriate. In the following, the major findings of the present finite element study will be presented. A schematic of the problem is given in Fig. 1.1, and details regarding the finite element formulation of the problem, the mesh design and specifications, and the boundary conditions, can be found in [12, 13] as well as in Part I [5] of this study. Note also that all computations are carried out with the Poisson's ratio $\nu = 0.3$, and all logarithmic values in the figures are based on the natural number e.

2. Quasi-static crack growth

2.1. Active plastic zones

We begin our discussion on crack-tip active plastic zone with a comparison to the result obtained by Narasimhan, Rosakis and Hall [11] using a nodal release finite element procedure. At the twentieth step of the nodal release, their solution is found to be in an approximate steady state, and is hence comparable with our steady state solution. Shown in Fig. 2.1 is the comparison for the crack-tip active plastic zone for a hardening elastic-plastic material with hardening exponent $n = 5$. Note that the coordinates are nondimensional; they are normalized by $(K/\sigma_0)^2$, where K stands for the far-field stress intensity factor. As expected, overall good agreement is observed. The slight difference can be attributed to the coarser mesh used in [11]. For example, since larger elements are used near the crack tip, the near-tip plastic zone boundary predicted in [11] lacks the detail at the crack tip. This also can be seen from comparisons of angular and radial variations of the near-tip fields in later subsections.

The progressive changes of the crack-tip active plastic zone with respect to n is illustrated in Fig. 2.2, also in normalized coordinates. As the level of strain hardening decreases (that is, as n increases), the plastic zone is seen to expand in the direction of crack growth and to contract in the perpendicular direction. For example, its horizontal size or width varies from $0.175(K/\sigma_0)^2$ for $n = 2$ to $0.229(K/\sigma_0)^2$ at $n = 10$, while its vertical size or height changes from $0.177(K/\sigma_0)^2$ for $n = 2$ to $0.128(K/\sigma_0)^2$ at $n = 10$. It is noted that the angular extent of the active plastic zone decreases as n increases, and that there is no secondary active plastic zone behind the crack tip. This will be further elaborated later on.

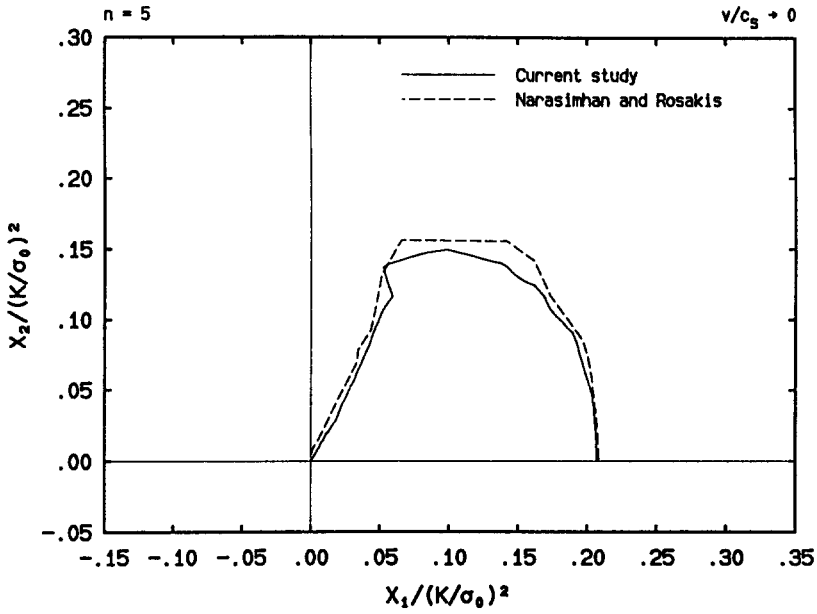

Fig. 2.1. A comparison of the crack-tip active plastic zone in normalized coordinates with that of Narasimhan, Rosakis and Hall [11] for $n = 5$, with the crack tip situated at the origin.

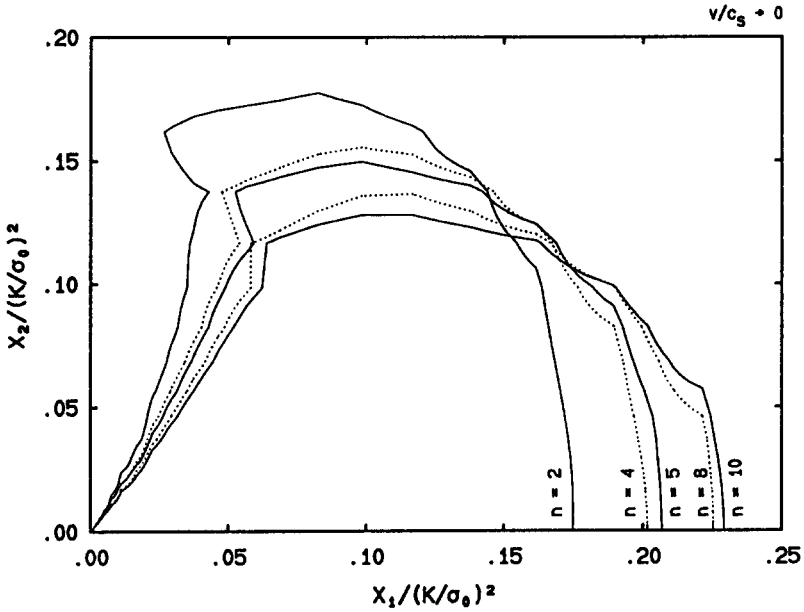

Fig. 2.2. The effect of hardening on the crack-tip active plastic zone in normalized coordinates, with the crack tip situated at the origin.

2.2. *Angular field variations*

The angular variations of the near-tip stress and velocity fields are presented in this subsection. We will first look at a comparison of stress variations for $n = 5$ (Fig. 2.3) with those obtained in [11]. Since stress values from the present study and [11] are taken along different contours

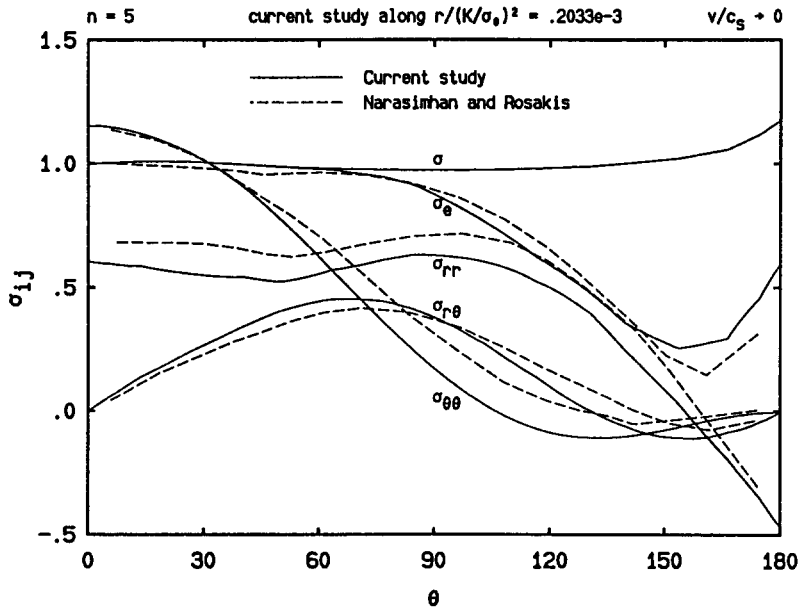

Fig. 2.3. Angular variations of the polar stress components, the effective stress σ_e, and the flow stress σ for $n = 5$, normalized such that $\sigma_e = 1$ at $\theta = 0$, with comparison to the solution by Narasimhan, Rosakis and Hall [11].

around the crack tip, they will be normalized such that the von Mises effective stress σ_e equals one at $\theta = 0$. This is done to emphasize the angular dependence of the stresses. The comparison shows that, although the overall tendency of the two solutions is similar, their quantitative differences are quite large, which can be explained as follows.

First, as discussed later, stresses in hardening materials are strong functions of the radial distance to the crack tip. To minimize the radial dependence, circular contours around the crack tip must be used in order to extract realistic angular variations. To this end, we note that while circular paths are used in the present study, those employed in [11] are rectangular, which will certainly introduce any radial dependence into the angular variations. On the other hand, we note that in the case of ideal plasticity, the stresses are almost independent of the radial distance, and a similar comparison demonstrates a much better agreement (see Fig. 3(a) of [14]).

Second, the present study used a much more detailed mesh than the one used in [11]. For example, in the present study the ratio of the crack-tip active plastic zone size to that of the smallest near-tip element is about 16,000, whereas in [11] the ratio is only about 385. As a result, asymptotic field values can be taken from locations very close to the crack tip (at a distance about $0.2 \times 10^{-3}(K/\sigma_0)^2$ to the crack tip) in this study, while those from [11] are taken at locations about $0.2 \times 10^{-1}(K/\sigma_0)^2$ away from the crack tip. The effect of this near-tip mesh resolution can be further seen later in the comparison of radial field variations.

The influence of hardening on the angular stress variations are demonstrated in Figs. 2.4a and 2.4b, where stresses for various values of n are similarly normalized and are plotted against the angular coordinate θ. The slopes of the polar stress components σ_{rr} at $\theta = 0$ and $\sigma_{\theta\theta}$ at $\theta = 0$ and 180° are seen to be very close to zero. Large compressive radial stress σ_{rr} is observed behind the crack tip (see Fig. 2.4a) for all n values investigated, which indicates a tendency of reverse plastic loading near the crack surface. However, this tendency is not strong enough to reach yielding since the effective stress σ_e is always smaller than the current yield stress or flow stress σ. Of

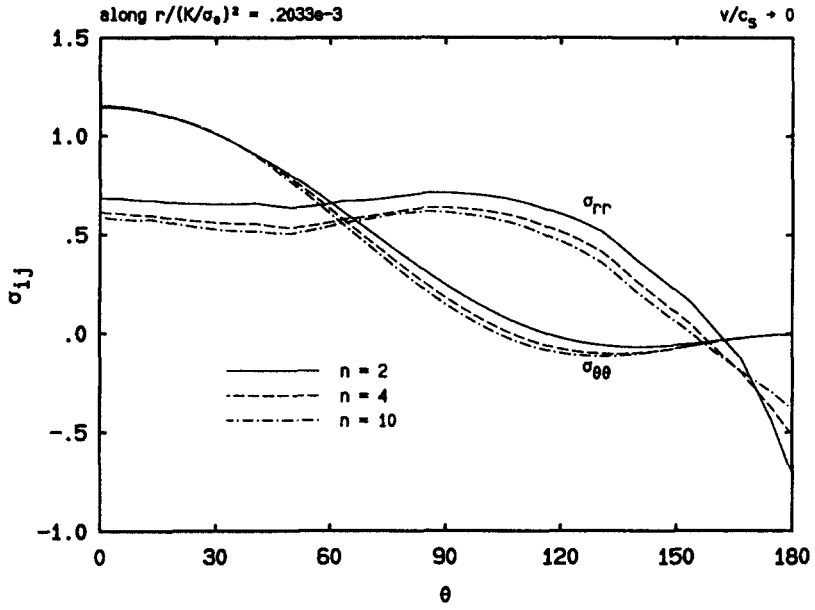

Fig. 2.4a. The effect of hardening on the angular variations of the polar stress components σ_{rr} and $\sigma_{\theta\theta}$, normalized such that the effective stress $\sigma_e = 1$ at $\theta = 0$.

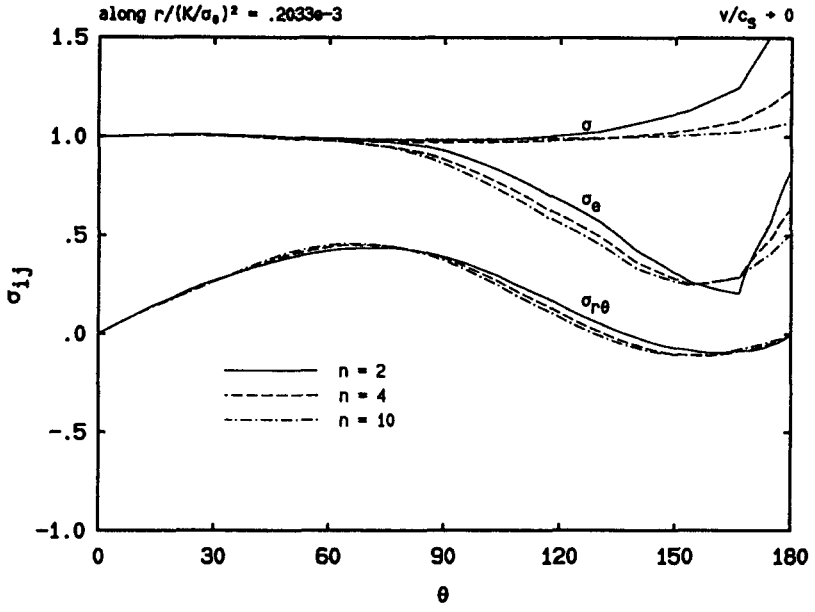

Fig. 2.4b. The effect of hardening on the angular variations of the polar stress component $\sigma_{r\theta}$, the effective stress σ_e, and the flow stress σ, normalized such that $\sigma_e = 1$ at $\theta = 0$.

course, this also suggests that if yielding is actually achieved near the crack flank, it must be limited to an extremely small range near $\theta = 180°$, so that one can in fact neglect its existence. It is also noted that the traction-free condition $\sigma_{\theta\theta} = \sigma_{r\theta} = 0$ along the crack surface and the symmetry condition $\sigma_{r\theta} = 0$ along the prospective crack line $\theta = 0$ are well satisfied, which is a major sign of convergence of the finite element computation based on the Eulerian formulation.

As discussed in [5] for the case of linear hardening, the angular extent of the crack-tip active plastic zone can be estimated by locating the elastic unloading angle at which the effective stress σ_e deviates from the flow stress σ. To do that numerically, an error tolerance must be specified for the relative difference between σ_e and σ. For example, using the error tolerance 0.77×10^{-2}, which was obtained in [5] from comparison with an asymptotic analysis for a particular linear hardening material and used for other linear hardening solids, the unloading angle is found to vary from 70° for $n = 2$ to 55° for $n = 10$. It must be pointed out that this estimation procedure is quite sensitive to the choice of the error tolerance, and for different hardening materials the accuracy of estimations is expected to be different.

The effect of hardening on the angular variations of the velocity field is shown in Fig. 2.5, where the velocity components are normalized such that $v_1 = -1$ at $\theta = 0$. It is found that for each individual material the qualitative behavior of the velocity components is very similar to that for the case of linear hardening, but the relative variations of the velocity curves for materials with different levels of strain hardening are different (compare Fig. 2.5 with Fig. 3.6 of [5]). This is believed to be due to the difference in the type of strain hardening.

2.3. *Radial field variations*

To lay out a clear yet concise picture of the radial variations of the near-tip field quantities, in this subsection and later for the case of dynamic crack propagation, many observations will be presented without illustration. When figures are included for some field quantities along certain radial directions, they should be regarded as being typical of the radial variations of similar field quantities and along other radial lines. Most radial variations will be plotted in nondimensional, special logarithmic coordinates (in order to compare with the predictions of asymptotic analyses [1–4]), but counterpart plots in original regular coordinates have been documented in [13] as

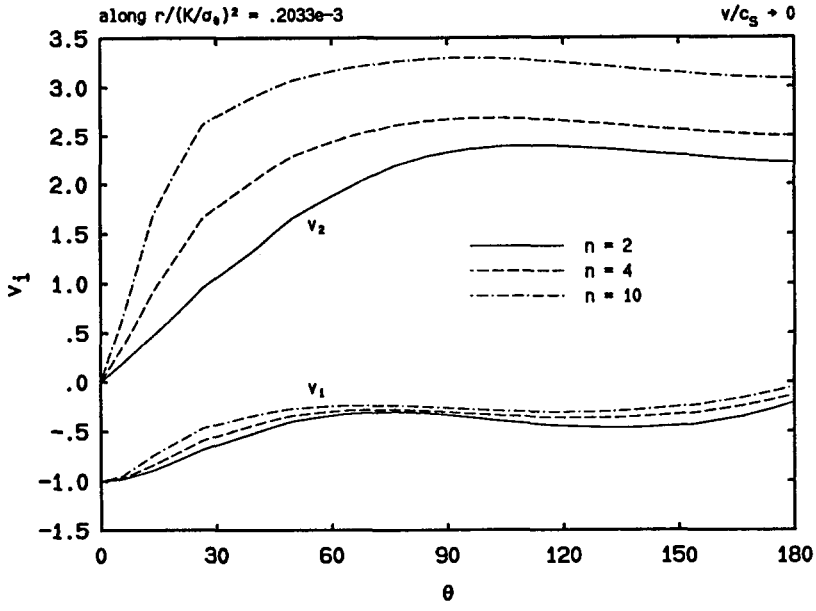

Fig. 2.5. The effect of hardening on the angular variations of the Cartesian velocity components, normalized such that $v_1 = -1$ at $\theta = 0$.

ready reference. All data are taken at locations five elements away from the crack tip and only one data point is used in each element.

Similar to the case of linear hardening, near-tip stresses and strains are found to be strong functions of r, the radial distance to the crack tip. As r approaches zero, the values of the stresses and strains rise rapidly, indicating stress and strain singularities at the crack tip. If the singularities are of the logarithmic type, as predicted by asymptotic analyses [1–4] for some cases of quasi-static crack growth (but not under plane stress conditions), straight lines must be observed if the near-tip stress or strain variations are plotted against r in an ln (stress or strain) vs. ln (ln(r)) coordinate. To this end, the radial variations of the stress component σ_{22} along the radial line $\theta = 0$ are shown in Fig. 2.6 for various values of n, where appropriate normalizations have been used and the data points on the far right are nearest the crack tip. Undoubtedly, we observe nearly straight lines. Hence, and with similar observations about other stress components, we conclude that stresses indeed behave as $[\ln(R_0/r)]^s$ $(s > 0)$ as $r \to 0$, where R_0 is a length scaling parameter. It is seen that as n increases, both s (the slope of the straight lines) and the magnitudes of the stress components decrease, which suggests that stress singularity at the crack tip is weaker for lower hardening materials. Note that the scaling parameter $(K/\sigma_0)^2$ used in Fig. 2.6 and in later figures is a choice of convenience and is otherwise arbitrary. There are some difficulties in determining the actual scaling parameter R_0, and a detailed discussion about this is deferred until a later time.

Comparisons with the solutions of Narasimhan, Rosakis and Hall [11], which were obtained using a different finite element technique, are shown in Figs. 2.7a, for stress components σ_{11} and σ_{22}, and 2.7b, for plastic strain component ε^p_{22}. Radial variations in both figures are along the prospective crack line $\theta = 0$. As expected, the two solutions agree very well at locations sufficiently away from the crack tip. But it is clear that the values of σ_{11} and ε^p_{22} obtained in [11] deviate from those of the present study at locations closer to the crack tip; in fact, that of σ_{11}

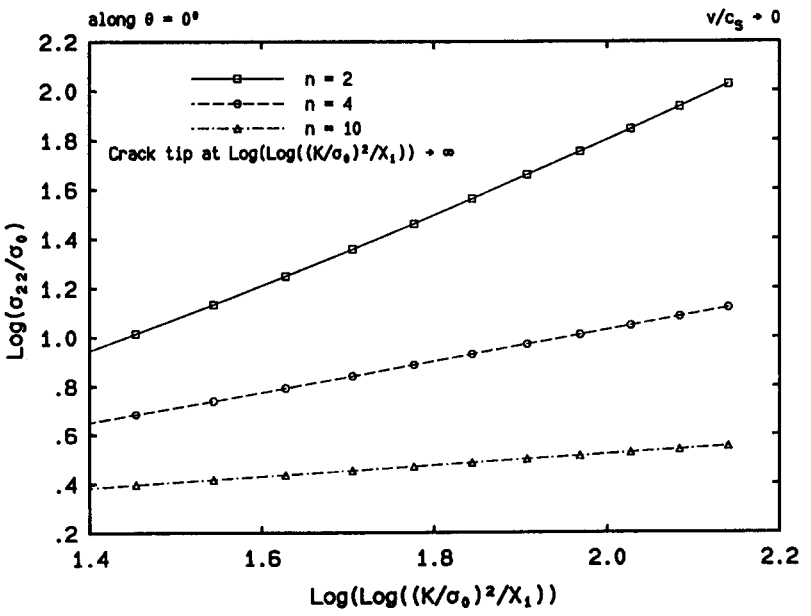

Fig. 2.6. Radial variations of the stress component σ_{22} along the prospective crack line in normalized, special logarithmic coordinates.

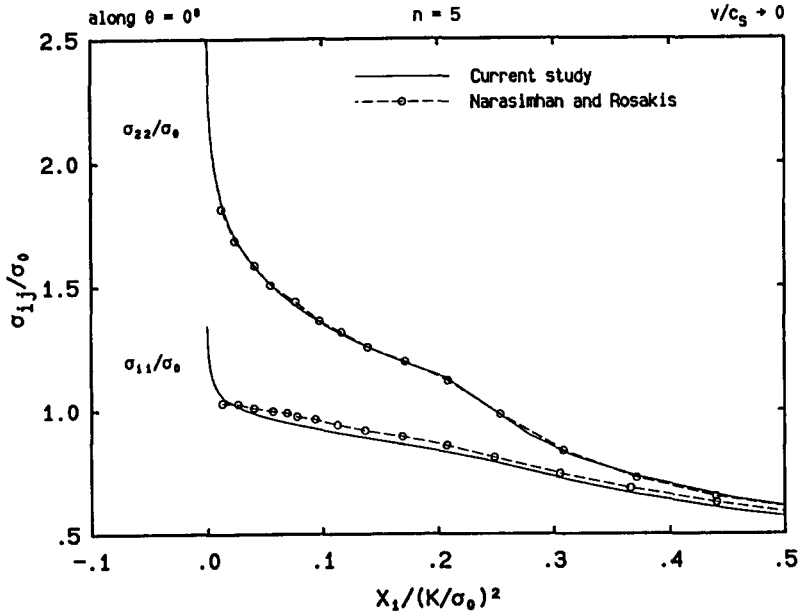

Fig. 2.7a. Radial variations of the stress components σ_{11} and σ_{22} along the prospective crack line for $n = 5$, compared with those of Narasimhan, Rosakis and Hall [11].

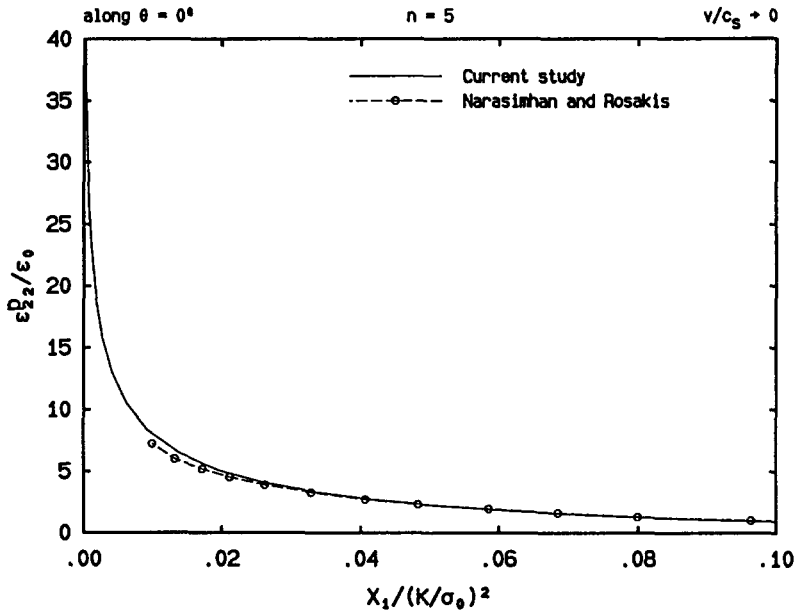

Fig. 2.7b. The radial variation of the plastic strain component ε^p_{11} along the prospective crack line for $n = 5$, compared with that of Narasimhan, Rosakis and Hall [11].

from [11] simply missed the characteristic singular feature near the crack tip. This again is caused by the strong radial dependence of the field quantities and by the use of a coarse finite element mesh in [11]. A similar comparison of stress variations in the case of ideal plasticity, for which stresses are weakly dependent on the radial distance, showed very good agreement (see Fig. 3(b) of [14]).

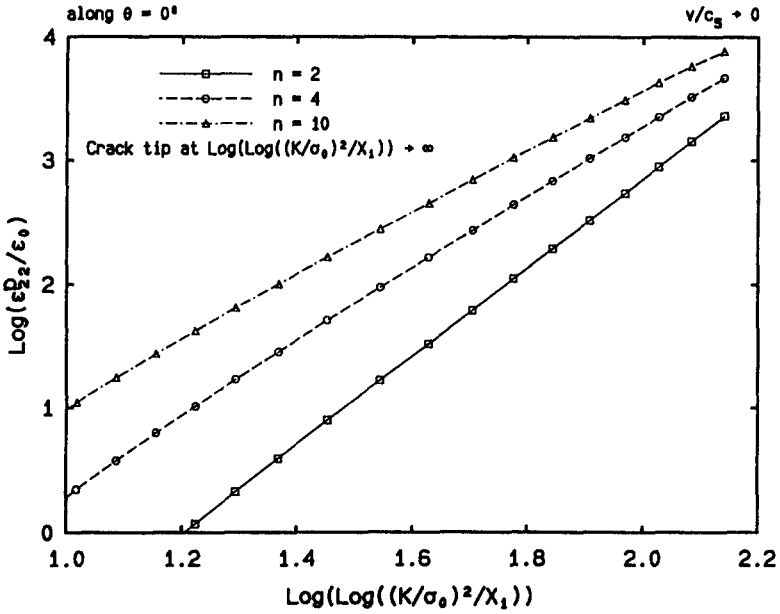

Fig. 2.8. Radial variations of the plastic strain component ε_{22}^{p} along the prospective crack line in normalized, special logarithmic coordinates.

The radial variations of the near-tip plastic strain components bear similar singular features at the crack tip as those of the stresses. As shown on Fig. 2.8 in the special logarithmic coordinates, the strain curves for materials with different power-law hardening exponents all appear as straight lines. That is, the plastic strains behave as $[\ln(R_0/r)]^s$ ($s > 0$) as the crack tip $r = 0$ is approached, where the length scaling parameter R_0 and the singularity exponent s are not necessarily the same as those for the stresses. It is clear from Fig. 2.8 that s here decreases as n increases, which implies that the crack-tip strain singularities are weaker for materials with weaker strain hardening.

Earlier in the paper, it was pointed out that the studies by Gao and his co-workers [1–4] obtained asymptotic solutions with stress and strain singularities of the type revealed by the present numerical study for quasi-static crack growth under mode I plane stress conditions (for which there are yet no asymptotic analyses). The asymptotic analyses in [1–4] also derived explicit relations between s and n, which, for the case of mode I plane strain, are $1/(n-1)$ for stresses and $n/(n-1)$ for strains. To firmly establish the existence and explore the usefulness of the crack-tip stress and strain singularities, it is desirable to estimate the singularity exponent s, as well as the range of singularity dominance, from a detailed full-field numerical study, such as the present one, and to compare with those predicted by corresponding asymptotic analyses. However, despite the success of such estimations in [5] for linear hardening materials, it is found that there are inherent difficulties in repeating the estimations here for the type of singularities for power-law hardening materials, and accordingly meaningful estimates cannot be obtained. The difficulties, it is believed, mostly stem from the fact that a singularity of the form $[\ln(R_0/r)]^s$ is a very weak singularity. Since the logarithmic expression is precise only asymptotically at $r = 0$, the estimate for s will depend on the scaling parameter R_0. It can be shown that this dependence is negligible only when the data points are extremely close to the origin.

On the other hand, if s is known, say, from an asymptotic analysis, then one can proceed to estimate the value of R_0 from a full-field numerical solution. Again, due to the fact that $[\ln(R_0/r)]^s$ is a weak singularity, and that different stress and strain components may have different zones of singularity dominance, the estimated values of R_0 will be different for different stress and strain components if the data points are not arbitrarily close to the crack tip. Nonetheless, we have computed, for each nonzero stress and plastic strain component along $\theta = 0$, an estimate of R_0 from data taken from the sixth to the tenth elements (the crack tip is at the lower-left corner of the first element). We also assume that s equals $1/(n-1)$ for stresses and $n/(n-1)$ for plastic strains. For comparison purposes, we express R_0 as $\beta(K/\sigma_0)^2$ and denote the values of the coefficient β estimated from σ_{11}, σ_{22}, ε_{p11} and ε_{p22} as, respectively, β_1, β_2, β_3 and β_4. Results of the estimations are listed in Table 2.1.

We now present results regarding radial variations of the near-tip displacement field. For $n = 5$, the crack-tip opening displacement δ, which is twice the vertical displacement u_2 along the crack surface, obtained in this study is compared with that of [11]. As shown in Fig. 2.9, the value of δ predicted in [11] is slightly larger than ours, which again is attributed to the use of a coarser finite element mesh in [11].

Table 2.1 Values of R_0, expressed as $\beta(K/\sigma_0)^2$, for quasi-static crack growth

η	β_1	β_2	β_3	β_4
2	0.165	0.077	0.205	0.042
4	0.081	0.031	0.520	0.023
5	0.079	0.028	0.945	0.022
8	0.089	0.027	5.34	0.022
10	0.099	0.026	13.2	0.022

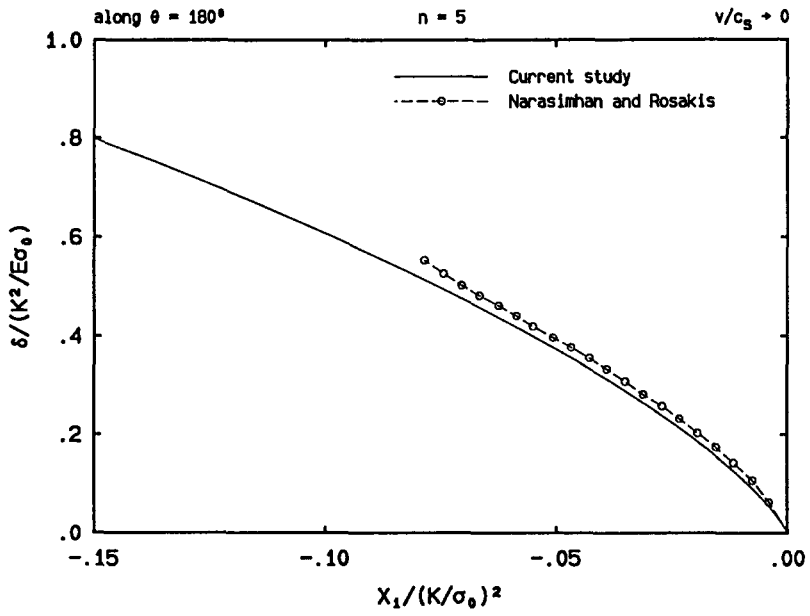

Fig. 2.9. The crack opening displacement δ (twice the vertical displacement u_2 along the crack surface) in normalized coordinates, compared to the finite element solution by Narasimhan, Rosakis and Hall [11].

The effect of hardening on the crack opening profile for power-law hardening materials has the same trend as that for linear hardening solids. That is, as the level of hardening decreases (n increases), the crack opening displacement is found to decrease accordingly.

3. Dynamic crack propagation

3.1. Active plastic zones

When the crack propagation speed is moderate, say $v = 0.3c_s$, where c_s is the elastic shear wave speed of the material, the effect of hardening on the size and shape of the crack-tip active plastic zone is qualitatively the same as that for quasi-static crack growth. For example, as shown in Fig. 3.1, the crack-tip plastic zone elongates horizontally and shortens vertically as n increases. For $n = 2$, the width and height of the plastic zone are, respectively, $0.182(K/\sigma_0)^2$ and $0.187(K/\sigma_0)^2$, while for $n = 10$, they are respectively $0.232(K/\sigma_0)^2$ and $0.152(K/\sigma_0)^2$.

However, when the crack speed is sufficiently high (so is inertia), say $v = 0.4c_s$, there exist certain different features. First, as n increases, the near-tip angular extent of the crack-tip active plastic zone is also found to increase, although slightly, which is contrary to that observed when crack speed is low. Second, when n is larger or equal to 4, a secondary active plastic zone is detected along the crack surface, whereas when v is smaller, no such reverse yielding zone is observed along the crack surface for all n values considered. We will get back to the above findings later on when we discuss the angular variations of the near-tip stress field.

The effect of crack propagation speed on the crack-tip active plastic zone has several general features. The results of this study show that as m increases, where m is the ratio of v to c_s and is named the Mach number, the height and the angular extent of the active plastic zone increase

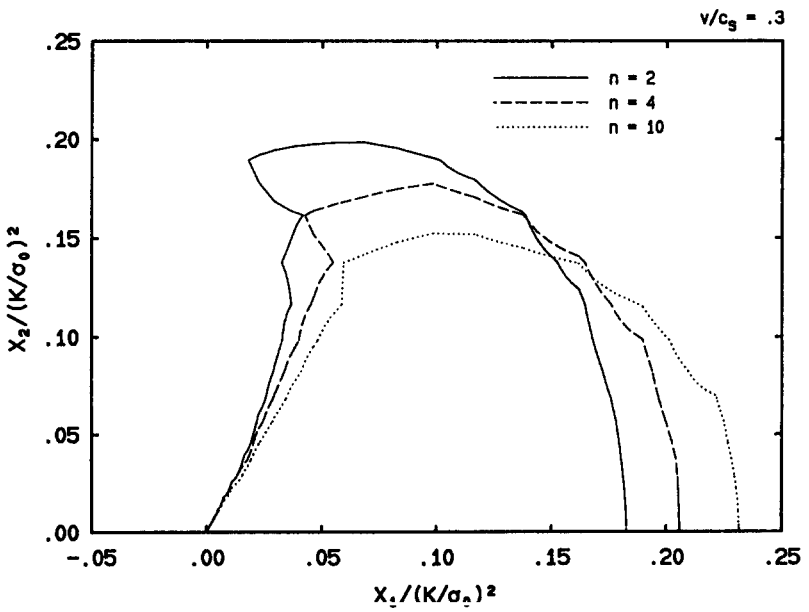

Fig. 3.1. The effect of hardening on the crack-tip active plastic zone for $v/c_s = 0.3$ in normalized coordinates, with the crack tip situated at the origin.

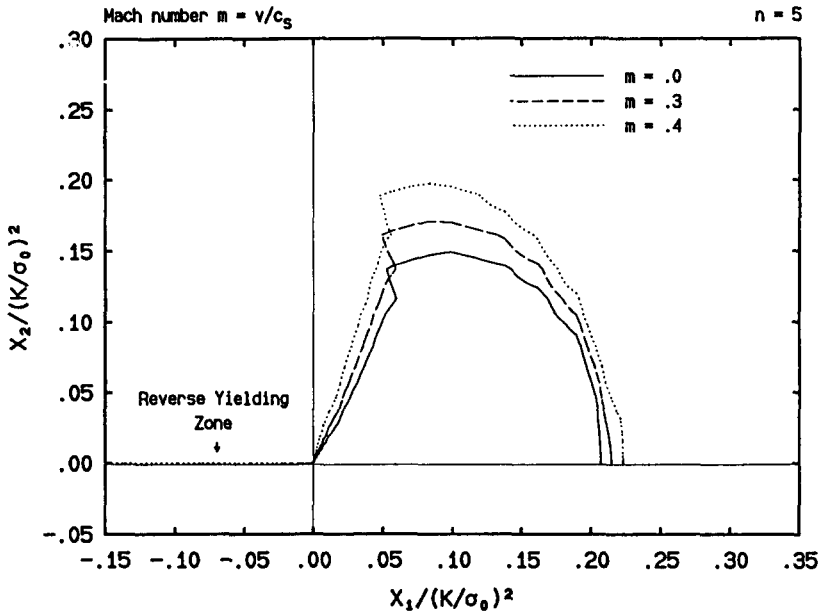

Fig. 3.2. The effect of crack propagation speed on the crack-tip active plastic zone for $n = 5$ in normalized coordinates, with the crack tip situated at the origin.

likewise. However, as m increases the width of the plastic zone is found to undergo a transition – it first increases when n is small and then decreases, although lightly, when n is sufficiently large. Figure 3.2 depicts the inertia effect for the case of $n = 5$. Again we can see that a secondary yielding zone is emerging along the crack flank when $m = 0.4$. Combining the above with similar observations from Part I of this study for the case of dynamic crack propagation in linear hardening solids, we conclude that when the crack speed is sufficiently high and when the material (whether linear hardening or power-law hardening) is almost ideally plastic (non-hardening), a small, secondary active plastic zone will develop along the crack surface, which is consistent with the findings for elastic-perfectly plastic materials (see [14]).

3.2. Angular field variations

The angular variations of the near-tip stress and velocity components for power-law hardening materials are very similar to those for linear hardening solids. As such, only a few representative figures will be included here. Figures 3.3a and 3.3b, for the case of $n = 10$, illustrate several common features of the stress variations in hardening materials during *rapid* dynamic crack propagation. Note that all stress quantities are normalized by the initial yield stress σ_0. When the crack speed is equal to 40 percent of the elastic shear wave speed, we observe that kinks in the angular variations of polar stress components σ_{rr} and $\sigma_{r\theta}$ are present near where elastic unloading is taking place (which is marked by the point of deviation of the effective stress σ_e from the current flow or yield stress σ). No kink is found for the angular variations of $\sigma_{\theta\theta}$. Moreover, the appearance of the kinks in σ_{rr} and $\sigma_{r\theta}$ near the elastic unloading angle is accompanied by the emergence of a secondary active plastic zone along the crack surface, which is indicated by the coincidence of σ_e with σ near $\theta = 180°$.

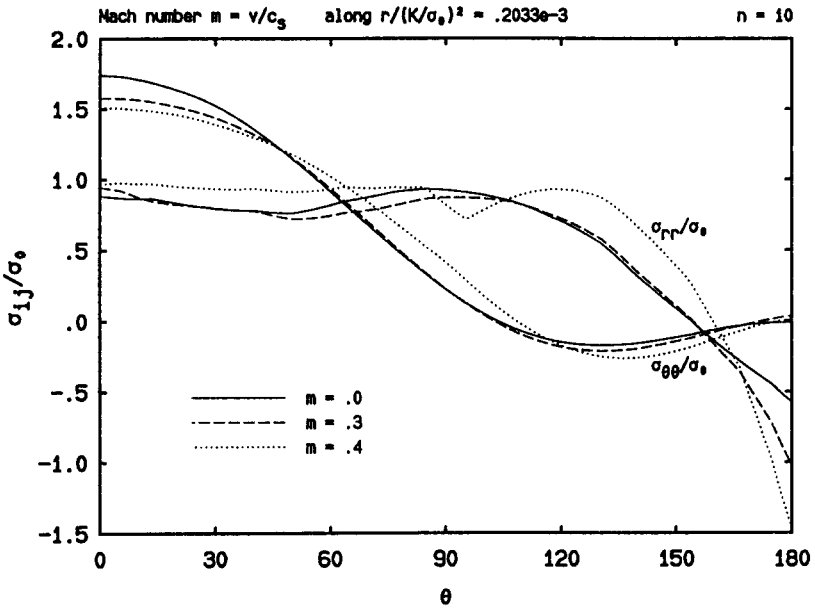

Fig. 3.3a. The effect of crack propagation speed on the angular variations of the polar stress components σ_{rr} and $\sigma_{\theta\theta}$ for $n = 10$, in normalized form.

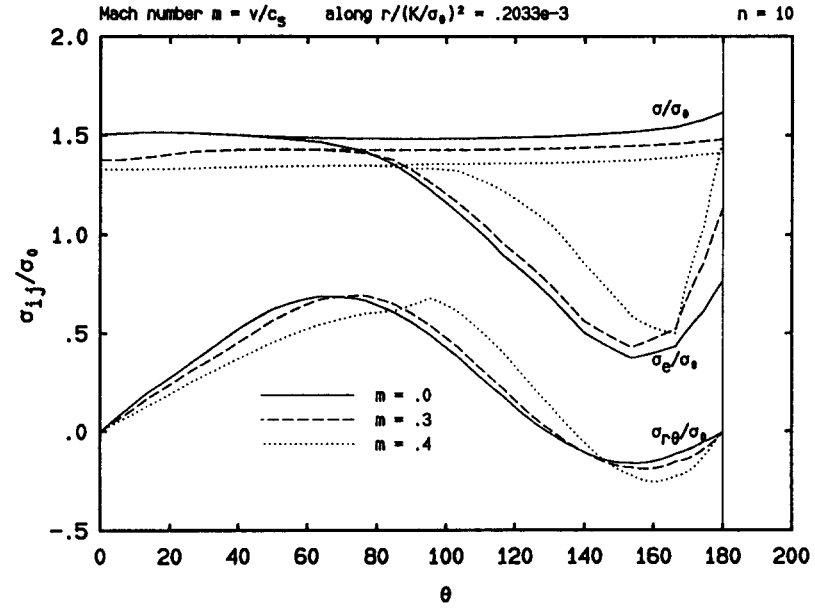

Fig. 3.3b. The effect of crack propagation speed on the angular variations of the polar stress component $\sigma_{r\theta}$, the effective stress σ_e, and the flow stress σ for $n = 10$, in normalized form.

The angle at which elastic unloading occurs can be estimated following the procedure stated earlier for quasi-static crack growth, which was discussed in the first part of this study [5]. By taking the same error tolerance, the unloading angle at $m = 0.3$ is found to be 76.9° when $n = 2$ and 72.4° when $n = 10$, whereas at $m = 0.4$, it is 82.3° when $n = 2$ and 85.9° when $n = 10$, with opposite tendency.

In the following, a qualitative comparison of the findings of the present study with those of a first-order asymptotic analysis by Zhang and Gao [4] is presented. However, a similar quantitative comparison is found to be difficult. We note that it is concluded in [4] that the angular variations of the crack-tip fields do not depend on the power-law hardening exponent n. The argument made in [4] is that very near the crack tip the values of the plastic strains are so high that the effective stress and strain relationship is basically that of an elastic-perfectly plastic solid, no matter what n is. As a result, the angular field variations must be the same as those for elastic-perfectly plastic materials. To this end, we note that today the only asymptotic analysis for dynamic crack growth under mode I plane stress in ideally plastic solids is given by Gao [15], and a detailed comparison of this study with a full-field numerical solution by the current authors has been given in [14]. That comparison reveals many similarities as well as differences between the two solutions, and there are still issues not resolved. The differences are attributed to the lack of dominance at the crack tip for the dynamic asymptotic solution, which confirms the result of an earlier analysis by Freund and Douglas [16] for mode III.

The argument made in [4] is in many aspects consistent with our observations. First it is indeed observed that the strains tend to grow without bound as the crack tip is approached, hence at the crack tip the slope of the power-law effective stress-strain curve is approximately zero, identical to that of an ideally plastic solid. Then, as predicted by the asymptotic solution of Gao [15] for crack growth in elastic-perfectly plastic materials, kinks do appear in the near-tip angular stress variations, which in fact can be seen for both linear and power-law hardening solids. However, there are also differences and open issues. For example, our full-field numerical study shows that the dependence of the angular stress variations on n is in general not negligible, and kinks appear only when the crack speed is very high and for materials without much hardening. Further, to say that the angular field variations are the same as those for ideally plastic solids *because* the strains are infinite, is to limit the validity of the asymptotic solution to a tiny crack-tip region that serves no practical purpose. We point out again that the angular stress variations of Gao [15] do not agree quantitatively with those obtained in this study.

Finally, the angular variations of the Cartesian velocity components v_1 and v_2 are shown in Fig. 3.4 for $m = 0.3$ and various n values, where a normalization is used such that $v_1 = -1$ at $\theta = 0$. The conclusion is that the variations will have different tendencies from those of quasi-static crack growth only when both m and n are sufficiently large.

3.3. Radial field variations

In this subsection we first briefly describe and discuss how n and m influence the radial variations of the near-tip stress and deformation fields. Then we proceed to illustrate the type of stress and strain singularities at the crack tip, compare with the prediction of the asymptotic study by Zhang and Gao [4], and, based on an earlier, similar discussion, further analyze the difficulties in estimating certain singularity parameters by least-square fitting of the full-field results to the type of singularities demonstrated above.

We start by noting that all stress and plastic strain components tend to rise continuously and rapidly as the crack tip is approached, indicating singularities there. At a certain Mach number m, the magnitudes of these near-tip quantities along $\theta = 0$ and at $r/(K/\sigma_0)^2$, a fixed normalized distance to the crack tip, decrease as n increases. On the other hand, for a certain n value and at a certain fixed normalized distance $r/(K/\sigma_0)^2$, the vertical normal stress and plastic strain

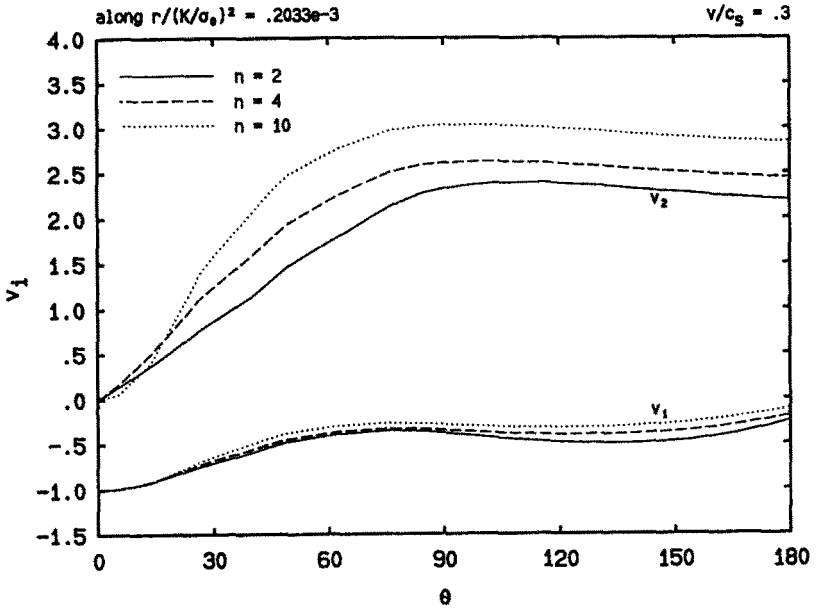

Fig. 3.4. The effect of hardening on the angular variations of the Cartesian velocity components for $v/c_s = 0.3$, normalized such that $v_1 = -1$ at $\theta = 0$.

components along $\theta = 0$ decrease as m increases, whereas their horizontal counterparts, which are always much smaller (especially when m is small), are seen to undergo transitions in their tendencies, depending on the values of n and $r/(K/\sigma_0)^2$ (the details are given in [13]).

Furthermore, similar to an observation in Part I of this study for crack growth in linear hardening solids [5], the effective plastic strain along the prospective crack line $\theta = 0$ is found to decrease near the crack tip as m increases when $r/(K/\sigma_0)^2$ is fixed, which is a result of the dominance of the vertical normal plastic strain component and its near-tip behavior. As stated in [5], the above feature can be utilized to derive K vs. v relations with the same qualitative trend as those measured on ductile metals and abstracted for ideally plastic solids (see [14]). In this light, it is also worth mentioning that observations can be made about the effects of crack propagation speed on the crack-tip opening displacement. These effects are similar for crack growth in all three classes of elastic-plastic materials: ideally plastic, linear hardening, and power-law hardening. The reader is referred to [5], [13] and [14] for details.

Regarding the type of singularities of the crack-tip fields during dynamic crack propagation, the radial stress and plastic strain variations are plotted in Figs. 3.5 through 3.8 in a set of normalized, special logarithmic coordinates, for various n and m values. It is clear from the figures that all stress and strain curves appear to be straight lines over a sizable region (some fraction of the size of the crack-tip active plastic zone). Therefore, both stress and plastic strain fields possess singularities of the type $[\ln(R_0/r)]^s$ ($s > 0$), where r is the radial distance to the crack tip; s is the singularity exponent and in general takes different values for stress and plastic strain components; and R_0 is a length scaling parameter.

As mentioned in the Introduction, the asymptotic analysis of Zhang and Gao [4] predicts that s is equal to $1/(n-1)$ for all stress components and $n/(n-1)$ for all strain components. Note that R_0 is not obtainable through asymptotic analysis. Supposedly, one would be able to estimate s and R_0 from a full-field solution, such as the one from the present finite element study.

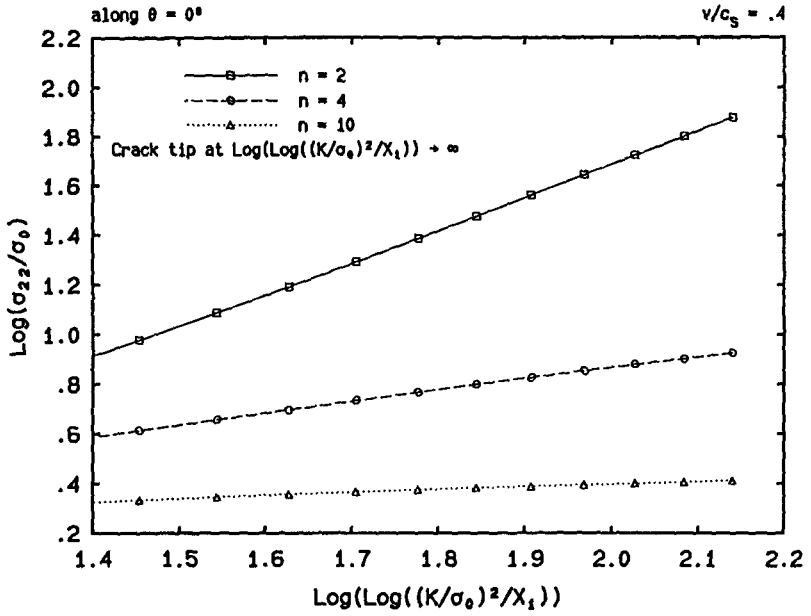

Fig. 3.5. Radial variations of the stress component σ_{22} for $v/c_s = 0.4$ along the prospective crack line in normalized, special logarithmic coordinates.

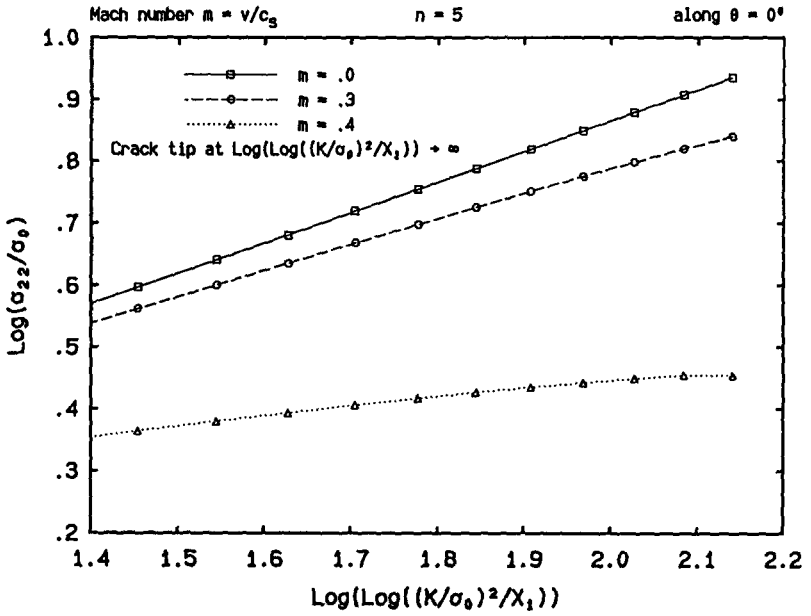

Fig. 3.6. Radial variations of the stress component σ_{22} for $n = 5$ along the prospective crack line in normalized, special logarithmic coordinates.

It is unfortunate however, that the type of first-order singularity (which is a weak singularity) predicted above is ill-conditioned for numerical estimation using least square fitting. This can be explained as follows. Firstly, as r approaches zero, the choice of the scaling parameter R_0 is *mathematically* nonunique, that is, the leading singularity term can be either $[\ln(R_1/r)]^s$ or $[\ln(R_2/r)]^s$, where R_1 and R_2 are any two reasonable positive numbers. Secondly, when stress or

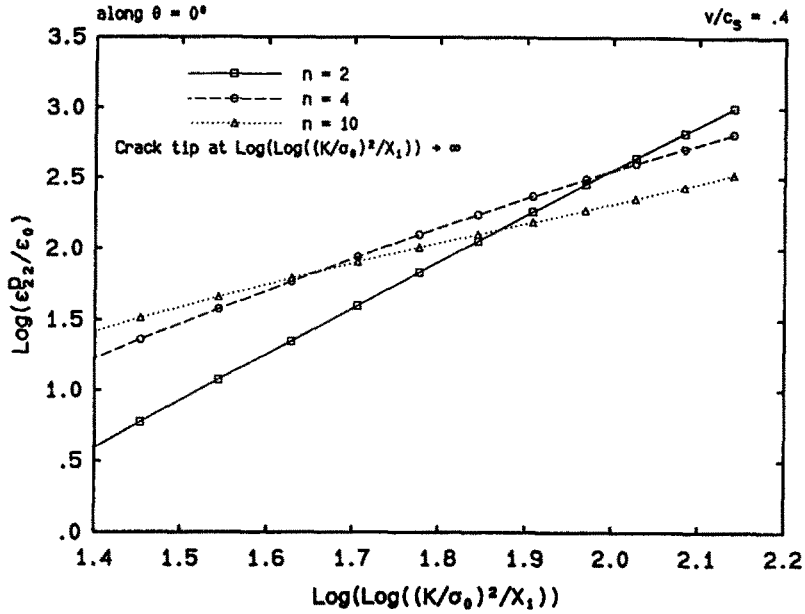

Fig. 3.7. The radial variation of the plastic strain component ε_{22}^{p} for $v/c_s = 0.4$ along the prospective crack line in normalized, special logarithmic coordinates.

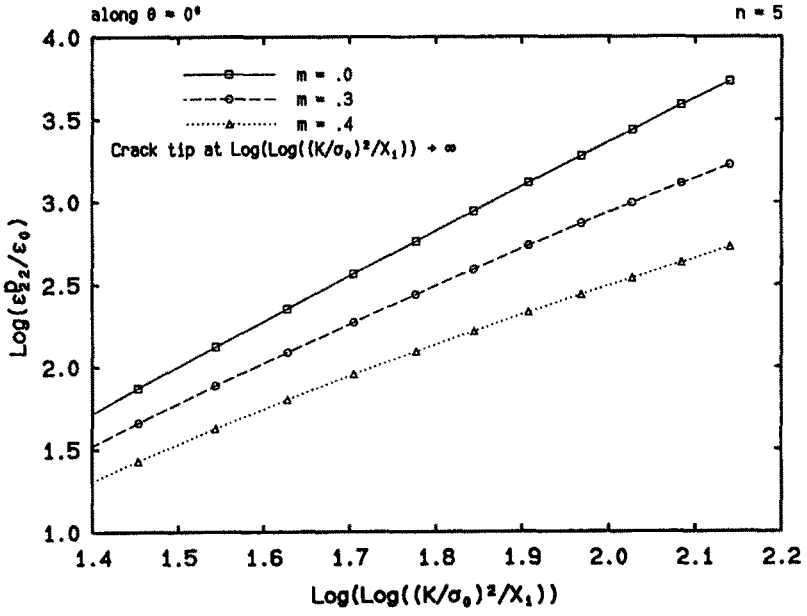

Fig. 3.8. The radial variation of the plastic strain component ε_{22}^{p} for $n = 5$ along the prospective crack line in normalized, special logarithmic coordinates.

strain values at different r are plotted in the special logarithmic coordinates, whether the curves will be straight or not will depend on the value used for R_0. For example, R_0 is taken as $(K/\sigma_0)^2$ in Figs. 3.5 through 3.8 for convenience since that was the original normalization in the finite element formulation. If a value very different from that is used in the figures, we will observe curved lines instead, although the singularity is still the same. Hence thirdly, the estimate for s

will be closely related to the value of R_0 (whether estimated or arbitrarily chosen), unless all data used are taken at locations extremely close to the crack tip (which is often not practical). As we can see, the above problems are really tangled together, and we were not able to come up with a practical and accurate numerical estimation procedure for s and R_0.

4. Closure

The results of a two-part finite element study of crack growth in hardening elastic-plastic solids have been presented. The study is carried out under mode I plane stress, steady-state, and small-scale yielding conditions. Details are given of the shape and size of the crack-tip active plastic zone, the asymptotic features of the near-tip stress and deformation fields, and the effects of hardening and crack propagation speed on the above quantities. In the case of linear hardening, the stresses and plastic strains possess power-type singularities at the crack tip, and their ranges of dominance are found to be quite large when compared to the size of the crack-tip active plastic zone. In the case of power-law hardening, however, the corresponding singularities are of the logarithmic type, and estimations for the singularity parameters involved, hence for the ranges of dominance of the stresses and strains, are shown to be difficult and impractical. The results also demonstrate that for a sufficiently low hardening material and at a sufficiently high crack speed, a secondary active plastic zone will exist in a narrow region along the crack surface, which is accompanied by the appearance of kinks in the angular variations of the radial and shear polar stress components. This distinctive behavior observable only at a high crack propagation speed is consistent with the findings for the limiting case of crack growth in nonhardening materials. The results of the present study can be used as a basis for higher-order asymptotic analysis, full-field experimental interpretations, and further numerical crack-growth simulations.

Acknowledgments

This study was made possible by an ONR grant through contracts N00014-85-K-0596 and N00014-90-J-1340. The finite element computation was carried out on CRAY X/MP and SCS-40 computers of the San Diego Supercomputer Center, which was made possible through the Presidential Young Investigator Award (NSF Grant MSM-84-51204) to AJR.

References

1. Y.C. Gao, X.T. Zhang and K.C. Hwang, *International Journal of Fracture* 21 (1983) 301–317.
2. Y.C. Gao and K.C. Hwang, in *Advances in Fracture Research, Proceedings of the 5th International Conference on Fracture*, Vol. 2, D. Francois et al. (eds.), (1981) 669–682.
3. Y.C. Gao and S. Nemat-Nasser, *Mechanics of Materials* 2 (1983) 305–317.
4. Z. Zhang and Y.C. Gao, *Acta Mechanica Sinica* 4 (1988) 22–34.
5. X. Deng and A.J. Rosakis, *International Journal of Fracture* 57 (1992) 291–308.
6. R.H. Dean and J.W. Hutchinson, in *Fracture Mechanics: Twelfth Conference, ASTM STP 700*, American Society for Testing and Materials (1980) 383–405.
7. J. Christoffersen and J.W. Hutchinson, *Journal of the Mechanics and Physics of Solids* 27 (1979) 465–487.
8. P.S. Lam, 'Numerical Analysis of Stable Crack Growth in Elastic-plastic Materials in Small Scale and General Yielding', Ph.D. thesis, University of Illinois at Urbana-Champaign (1982).

9. X. Luo, X. Zhang and K. Hwang, in *Proceedings of ICF International Symposium on Fracture Mechanics* (Beijing), Science Press, Beijing, China (1984) 138–145.
10. E.P. Sorensen, *International Journal of Fracture* 14 (1978) 485–500.
11. R. Narasimhan, A.J. Rosakis and J.F. Hall, *Journal of Applied Mechanics* 54 (1987) 846–853.
12. X. Deng and A.J. Rosakis, *Finite Elements in Analysis and Design* 7 (1990) 181–191.
13. X. Deng, 'Dynamic Crack Propagation in Elastic-plastic Solids', Ph.D. thesis, California Institute of Technology, Pasadena, CA 91125 (1990).
14. X. Deng and A.J. Rosakis, *Journal of the Mechanics and Physics of Solids* 39 (1991) 682–722.
15. Y.C. Gao, *International Journal of Fracture* 34 (1987) 111–129.
16. L.B. Freund and A.S. Douglas, *Journal of the Mechanics and Physics of Solids* 30 (1982) 59–74.